Biochimica et Biophysica Acta 1847 (2015) 748–758

Contents lists available at ScienceDirect

Biochimica et Biophysica Acta

journal homepage: www.elsevier.com/locate/bbabio

Probing the Cl^--pumping photocycle of *pharaonis* halorhodopsin: Examinations with bacterioruberin, an intrinsic dye, and membrane potential-induced modulation of the photocycle

Takashi Kikukawa [a,*], Chikara Kusakabe [a], Asami Kokubo [a], Takashi Tsukamoto [b], Masakatsu Kamiya [a], Tomoyasu Aizawa [a], Kunio Ihara [c], Naoki Kamo [a], Makoto Demura [a]

[a] Faculty of Advanced Life Science, Hokkaido University, Kita-ku, Sapporo 060-0810, Japan
[b] Division of Pharmaceutical Sciences, Graduate School of Medicine, Dentistry, and Pharmaceutical Sciences, Okayama University, Kita-ku, Okayama 700-8530, Japan
[c] Center for Gene Research, Nagoya University, Chikusa-ku, Nagoya 464-8602, Japan

ARTICLE INFO

Article history:
Received 21 March 2015
Received in revised form 1 May 2015
Accepted 4 May 2015
Available online 8 May 2015

Keywords:
Halorhodopsin
Carotenoid
Light-driven chloride pump
Photocycle
Flash photolysis
Microbial rhodopsin

ABSTRACT

Halorhodopsin (HR) functions as a light-driven inward Cl^- pump. The Cl^- transfer process of HR from *Natronomonas pharaonis* (NpHR) was examined utilizing a mutant strain, KM-1, which expresses large amount of NpHR in a complex with the carotenoid bacterioruberin (Brub). When Cl^- was added to unphotolyzed Cl^--free NpHR–Brub complex, Brub caused the absorption spectral change in response to the Cl^- binding to NpHR through the altered electrostatic environment and/or distortion of its own configuration. During the Cl^--puming photocycle, on the other hand, oppositely directed spectral change of Brub appeared during the O intermediate formation and remained until the decay of the last intermediate NpHR′. These results indicate that Cl^- is released into the cytoplasmic medium during the N to O transition, and that the subsequent NpHR′ still maintains an altered protein conformation while another Cl^- already binds in the vicinity of the Schiff base. Using the cell envelope vesicles, the effect of the interior negative membrane potential on the photocycle was examined. The prominent effect appeared in the shift of the N–O quasi-equilibrium toward N, supporting Cl^- release during the N to O transition. The membrane potential had a much larger effect on the Cl^- transfer in the cytoplasmic half channel compared to that in the extracellular half channel. This result may reflect the differences in dielectric constants and/or lengths of the pathways for Cl^- transfers during N to O and O to NpHR′ transitions.

1. Introduction

Halorhodopsin (HR) is a membrane protein that functions as a light-driven chloride ion pump [1] and belongs to the microbial rhodopsins, including ion pumps, cation channels and light-sensors [2,3]. Like other microbial rhodopsins, HR consists of a bundle of seven transmembrane helices that surround the retinal bound to a specific lysine residue via a protonated Schiff base. The light-induced isomerization of retinal from the all-*trans* to 13-*cis* configuration triggers the cyclic photoreaction of HR called a "photocycle". This cycle includes the sequential formation and decay of several intermediates. During the cyclic reaction, HR translocates a Cl^- from the extracellular (EC) space to the cytoplasmic (CP) space [4,5]. This inward Cl^- transport is thought to contribute to maintaining a high salt concentration in the cell interior and/or supporting energy transduction by acting as part of the proton motive force in ATP synthesis [6–8].

After the original discovery of HR from an extreme haloarchaeon, *Halobacterium salinarum* [9], many HR homologues have been identified from different sources. However, most studies have been conducted using the original HR from *H. salinarum* and HR from *Natronomonas pharaonis* (NpHR), an extremely haloalkaliphilic archaeon. In their dark states, both HRs bind Cl^- in the vicinity of a Schiff base NH^+ which is oriented toward the EC side [10,11]. During the photocycle, this Cl^- is considered to move to the CP side over the Schiff base region and then to be released to the CP space. After that, another Cl^- is captured on the EC side, which subsequently occupies the primary Cl^- binding site [4,5]. These Cl^- transfers should occur by the formation of particular intermediates; however, the details are not fully defined. In contrast, for the well-studied proton pump bacteriorhodopsin (BR), sequential proton transfer steps are clearly associated with individual intermediates [12,13].

Based on visible absorption and electrogenicity kinetic studies, Váró et al. and Ludmann et al. proposed the following scheme for the NpHR photocycle: NpHR → K ↔ L_1 ↔ L_2 ↔ N ↔ O ↔ NpHR′ → NpHR [14,15]. The two L intermediates, L_1 and L_2, have the same absorption

Abbreviations: HR, halorhodopsin; EC, extracellular; CP, cytoplasmic; NpHR, HR from *Natronomonas pharaonis*; BR, bacteriorhodopsin; K_d, dissociation constant; Brub, bacterioruberin; CCCP, carbonyl cyanide m-chlorophenyl hydrazine; TPT, triphenyltin; DDM, n-dodecyl β-D-maltopyranoside.

* Corresponding author at: Faculty of Advanced Life Science, Hokkaido University, N10W8, Kita-ku, Sapporo 060-0810, Japan. Tel.: +81 11 706 3435; fax: +81 11 706 2771.
E-mail address: kikukawa@sci.hokudai.ac.jp (T. Kikukawa).

http://dx.doi.org/10.1016/j.bbabio.2015.05.002
0005-2728/

spectra (λ_{max} ~ 530 nm), meaning the transition between them is spectrally silent. Váró et al. noticed that, among all of the rate constants, only the O → NpHR′ and O → N accelerated with increasing Cl^- concentration. Thus, they concluded that the O intermediate is a Cl^--free form [14]. This conclusion is credible because of the following two facts: Only the O intermediate has a redshifted absorption spectrum and removal of Cl^- from NpHR in the dark shows redshift due to disappearance of electrical interaction of Cl^- and positively charged protonated Schiff base. The same conclusion was also reported using a transient grating experiment where the Cl^- diffusion signal was detected synchronously with the appearance of O [16]. Furthermore, FTIR spectroscopy suggested structural similarity between the O intermediate and the anion-free unphotolyzed state [17]. However, the previous flash-induced voltage measurements led to the conclusion that O does not appear in the Cl^- transport photocycle [18]. On the other hand, other voltage measurements detected large electrogenicity during O formation [15,19]. These data support the model that Cl^- release is associated with O formation.

Previously, we analyzed the photocycle of NpHR [20,21] according to the sequential irreversible model of Chizhov et al. [22]. This model describes the scheme without the reverse reaction as: $P_0 \rightarrow P_1 \rightarrow P_2 \rightarrow \ldots \rightarrow P_n \rightarrow P_0$, where P_0 represents the original NpHR before flash excitation and P_i ($i = 1$ to n) represents a kinetically defined state that may contain a few physically defined intermediates if their quasi-equilibrium attains during the photocycle. We analyzed the photocycle after the K intermediate due to the slow response of the apparatus and found that the photocycle after the K intermediate was described by four P_i ($i = 1$ to 4) states. The third state P_3 was a quasi-equilibrium between N and O [20,21]. This quasi-equilibrium was also reported in other studies where these two intermediates appear and decay over nearly the same time course [14,23]. O contains all-*trans* retinal [24]. For N, the retinal configuration is not fully defined. However, previous time-resolved FTIR study detected N-like intermediate and showed its retinal to be in a 13-*cis* form [25]. Thus, the quasi-equilibrium between N and O implies a very low barrier between them. In the P_3 state, this equilibrium shifts toward O with the decrease of Cl^- concentration, suggesting that the O intermediate is a Cl^- releasing state [20,21]. A similar Cl^- dependence was also reported by Chizhov and Engelhard [23]. From the Cl^- dependence of the N–O equilibrium, the dissociation constant of Cl^- (K_d) was estimated to be ~1 M [20,21]. P_4 is found to be a mixture of notable amount of NpHR′ and a faint amount of O [20]. This implies that NpHR′ forms from O and does not form from N. Fig. 1 schematically shows this photocycle together with the results of present study. This photocycle scheme is essentially the same with that of Ludmann et al. [15].

Previously, NpHR-overproducing strain KM-1 was generated by UV mutagenesis from *N. pharaonis* type strain DSM2160^T [26]. Although the amino acid sequence of NpHR was not altered in this strain, the overexpression of NpHR was caused through a point mutation in the bacteriorhodopsin activator homologue of *N. pharaonis*. NpHR in KM-1 forms unique trimmer structure, in which the carotenoid Brub binds to crevices between NpHR monomers [11]. The crystal structure of this trimmer unit is shown in Fig. 2. Carotenoids are known to exhibit absorption spectral changes depending on their electrostatic environment and configuration [27–30]. Furthermore, Brub in the KM-1 membrane was reported to change its absorption spectrum upon Cl^- binding to unphotolyzed NpHR [26,31]. Thus, Brub might change its spectrum in response to Cl^- movement during the photocycle. We performed flash-photolysis experiments for the KM-1 membrane fragment and analyzed the absorption spectral change of Brub. Detailed analysis according to the sequential irreversible model revealed that the spectral change occurred in response to the formation of O and, to a lesser extent, remained until decay of NpHR′. On the other hand, an oppositely directed spectral change was observed when Cl^- was added to Cl^--free NpHR in the dark state. Using cell envelope vesicles prepared from KM-1 cells we further observed that the interior negative membrane potential

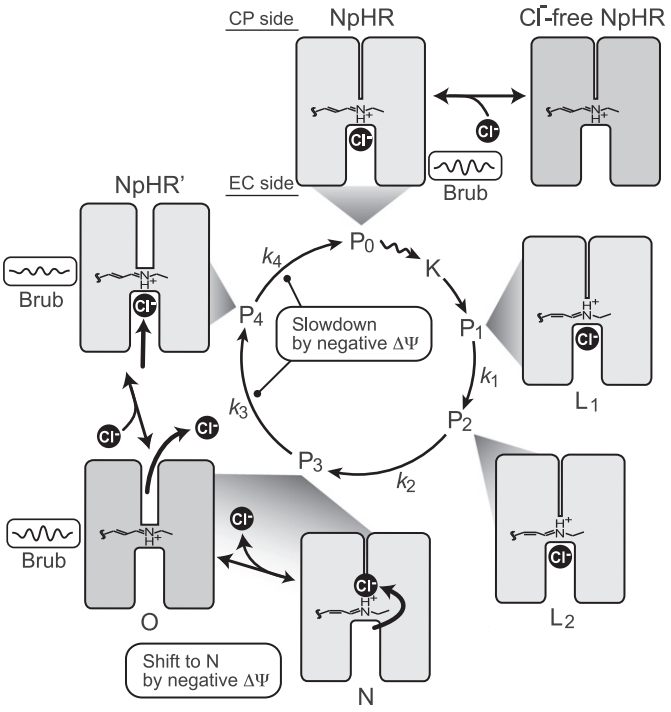

Fig. 1. Photocycle scheme of NpHR. Previously deduced scheme [20] is shown together with the results of present study. The P_4 state includes a small contribution of O, which is not shown here. The spectral change of Brub occurs at O and remains in NpHR′. The interior negative membrane potential ($\Delta\Psi$) shifts the N–O equilibrium toward N and slows down the decay of P_3 and P_4 states.

decreased O accumulation and slowed O decay. These results indicated that Cl^- release occurs during O formation, and the subsequent product is NpHR′ and not N.

2. Materials and methods

2.1. Growth conditions and cell disruption of KM-1

The growth medium was essentially the same as in Hirayama et al. [32]. The following two solutions were autoclaved separately. Solution A (per litter): Yeast Extract (Difco), 20 g; Casamino acids (Difco), 15 g; Na_3-citrate·$2H_2O$, 6 g; KCl, 4 g; $MgSO_4 \cdot 7H_2O$, 2 g; $MnCl_2 \cdot 4H_2O$, 0.72 mg; $FeSO_4 \cdot 7H_2O$, 100 mg; NaCl, 200 g. Solution B (per litter): NaCl, 200 g; $Na_2CO_3 \cdot 10H_2O$, 100 g. After cooling to room temperature, equal volumes of each were mixed and then used for the growth medium. The cells were grown aerobically at 37 °C. Starter cultures in 5 mL of medium inoculated with a single colony were grown and were used to inoculate 4 L growths in a 5-L flask. Then, the cells in stationary phase were harvested and washed twice with a solution of 4 M NaCl and 50 mM HEPES, pH 7. They were then resuspended with 200 mL of the same solution, and completely frozen by immersing in liquid nitrogen. Thawed suspensions were used for the membrane isolation and vesicle preparation described below.

2.2. KM-1 membrane isolation

A thawed suspension was mixed with 9 volumes of distilled water including 5 mg of DNase I (Sigma), and stirred for 1 h at room temperature and then overnight at 4 °C. After removal of any large debris by centrifugation at 6400 *g* for 30 min, the supernatant was centrifuged at 178,000 *g* for 1 h. The precipitated membrane fractions were washed 6 times with distilled water and then suspended in 1% Tween 20. After gentle stirring for 1 h at room temperature, the membrane fractions

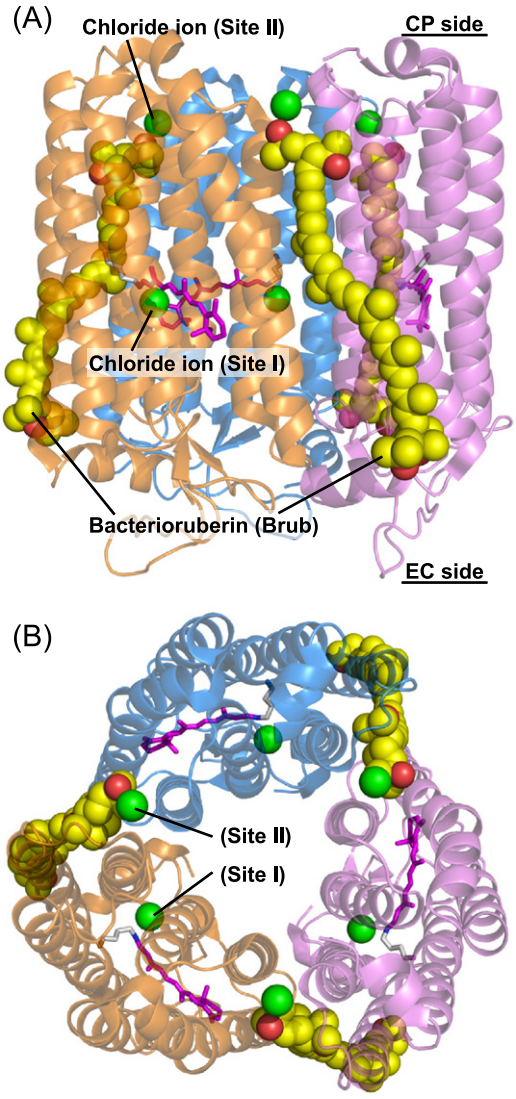

Fig. 2. Trimeric NpHR–Brub complex from KM-1 membrane. Side view of the complex (A) and the top view from the CP side (B) are shown. Retinal (magenta) shown in sticks binds to Lys256 via a protonated Schiff base, and Brub (yellow) shown in spheres binds to crevices between the NpHR monomers. The red spheres represent oxygen atoms. The green spheres represent chloride ions bound near the Schiff base (Site I) and bound to the site at the CP end of Brub (Site II). Two chloride ions are shown per NpHR monomer, thus, six chloride ions are shown per NpHR trimer. PDB code is 3A7K.

were collected by centrifugation, washed twice and finally suspended in 50 mM HEPES, pH 7.

2.3. KM-1 vesicle preparation and imposition of interior negative membrane potential

After adding 5 mg of DNase I, the thawed suspension of KM-1 cells was stirred for 1 h at room temperature and then overnight at 4 °C. The large debris was removed as described above and the supernatant was centrifuged at 178,000 *g* for 30 min. The collected vesicles were washed twice with 4 M NaCl and concentrated in a few milliliters of 4 M NaCl. To load KCl inside, the concentrated vesicle was diluted 1:100 into 3.3 M KCl containing 50 mM MOPS, pH 7, and then gently stirred for 1 h at room temperature. The vesicles were collected by centrifugation, resuspended in the same buffer, and gently stirred overnight at 4 °C. By centrifugation, the vesicles were then highly concentrated in the same buffer. The right-side-out ratio of the vesicles was approximately 70%, which was checked by the menadione/NADH method [33]. Furthermore, these vesicles showed high Cl^- pumping activity upon light irradiation. This activity was confirmed by the conventional pH electrode method [34]. To impose the K^+ diffusion potential, the concentrated vesicles were diluted 1:100 into a solution of 3.3 M NaCl containing 50 mM MOPS, pH 7. Then, valinomycin (Sigma) was added from a 0.1 mM ethanolic stock to a final concentration of 0.4 μM. The K^+ concentration outside the vesicle, $[K^+]_{out}$, was 1/100 of that inside the vesicle, $[K^+]_{in}$. Thus, the imposed membrane potential was −118 mV, as calculated by the Nernst equation:

$$\Delta\Psi_{mV} = -59 \log \left([K^+]_{in} / [K^+]_{out} \right) \quad (1)$$

The flash photolysis method was applied to these vesicles to examine the photocycle of NpHR in the presence of this interior negative membrane potential. In this method, the sample is irradiated by a repeated laser flash and a continuous monitoring light. Even in the absence of valinomycin, the interior negative membrane potential might be slightly imposed due to Cl^- transport of NpHR. For the measurements at a 0 mV membrane potential, thus, carbonyl cyanide m-chlorophenyl hydrazone (CCCP) and triphenyltin (TPT) were added (10 μM each) after the 1:100 dilution of the vesicles into 3.3 M NaCl.

2.4. Preparation of recombinant NpHR from E. coli cells

The expression and purification of histidine-tagged NpHR has been described in detail elsewhere [35]. Briefly, *E. coli* BL21(DE3) cells harboring the expression plasmid were grown at 37 °C in 2 × YT medium. The NpHR expression was induced by 1 mM isopropyl-β-D-thiogalactopyranoside in the presence of 10 μM all-*trans* retinal. After that, the cells were harvested and disrupted by a French press. The collected membrane fraction was then solubilized with n-dodecyl β-D-maltopyranoside (DDM) (Dojindo Lab, Kumamoto, Japan), and the solubilized NpHR was purified by Ni-NTA-agarose (Qiagen, Hilden, Germany) in the presence of 0.1% DDM. The samples were then replaced by the appropriate buffer solution by two passages over a PD-10 column (Amersham Bioscience, Uppsala, Sweden).

2.5. Absorption spectrum measurements

The absorption spectra were measured by UV1800 UV–VIS spectrophotometer (Shimadzu, Kyoto, Japan). For the measurements of the KM-1 membrane fragments, a small amount of DDM (0.01%) was added to prevent membrane aggregation. However, the obtained spectra still included large scattering artifacts. Thus, the Cl^--induced spectral changes were calculated after subtraction of scattering curves, which were determined by fitting two wavelength regions (340–360 and 725–750 nm) with $A + B/\lambda + C/\lambda^2$, where A, B and C denote the fitting parameters and λ denotes the wavelength. From the Cl^--induced absorbance changes (ΔA) of NpHR and Brub, the K_d of Cl^- was determined by fitting the data to the equation:

$$\Delta A = \Delta A_{max} \cdot [Cl^-]^n / (K_d{}^n + [Cl^-]^n) \quad (2)$$

where ΔA_{max} and n represent the maximum absorbance change and the Hill coefficient, respectively.

2.6. Flash-photolysis spectroscopy

The flash-photolysis apparatus equipped with Nd-YAG laser (532 nm, 7 ns) was described previously [36]. For all samples, the time-dependent absorbance changes were measured from 410 to 710 or 720 nm at 5 or 10 nm intervals. At each selected wavelength, 30–100 flashes were used to improve the signal-to-noise ratio. Data points on a logarithmic time scale were picked from the observed data for the plots and the following analysis. As described in the introductory section, we employed an irreversible sequential model based on Chizhov et al. [22]. The present analysis procedure was essentially the same as

our previous reports [20,36]. Briefly, the data obtained at all wavelengths were fit simultaneously to this model. Using the fitting results, the decay rate constants (k_i) of the kinetically defined P_i state and the absorption differences between P_i and the original state P_0 ($\Delta\varepsilon_i$) were calculated. To determine the absolute spectra of each P_i state, the absorption spectrum of the P_0 state is necessary. However, the spectrum of KM-1 membrane fragment includes strong absorption due to Brub. Thus, we used the spectrum of NpHR purified from *E. coli* in 10 mM MOPS, pH 7, containing 0.1% DDM and 1 M NaCl. This spectrum still includes background scattering and absorption due to the aromatic residues. Thus, the pure retinal spectrum was extracted by spectral decomposition as described previously [20,36] and was then used as the spectrum of P_0. By adding this retinal spectrum to the absorption difference ($\Delta\varepsilon_i$), the absolute spectra of each P_i state were obtained.

3. Results

3.1. Cl^- induced Brub spectral change in the dark state

The membrane fragments from KM-1 are claret colored due to two pigments, Brub and NpHR. In the absorption spectrum (Fig. 3A inset), the characteristic sharp peaks of Brub appeared at approximately 450–550 nm and the band from NpHR appeared at approximately 600 nm. NpHR is known to show a spectral blueshift (λ_{max}: 600 → 580 nm) upon Cl^- binding at the primary site (denoted as "Site I" in Fig. 2) in the vicinity of the Schiff base. Cl^- titrations showed that Brub also changes its absorption spectrum [26,31]. Probably, Brub responds to the Cl^--binding to the Site I through changes in its electrostatic environment and/or conformational changes of NpHRs. However,

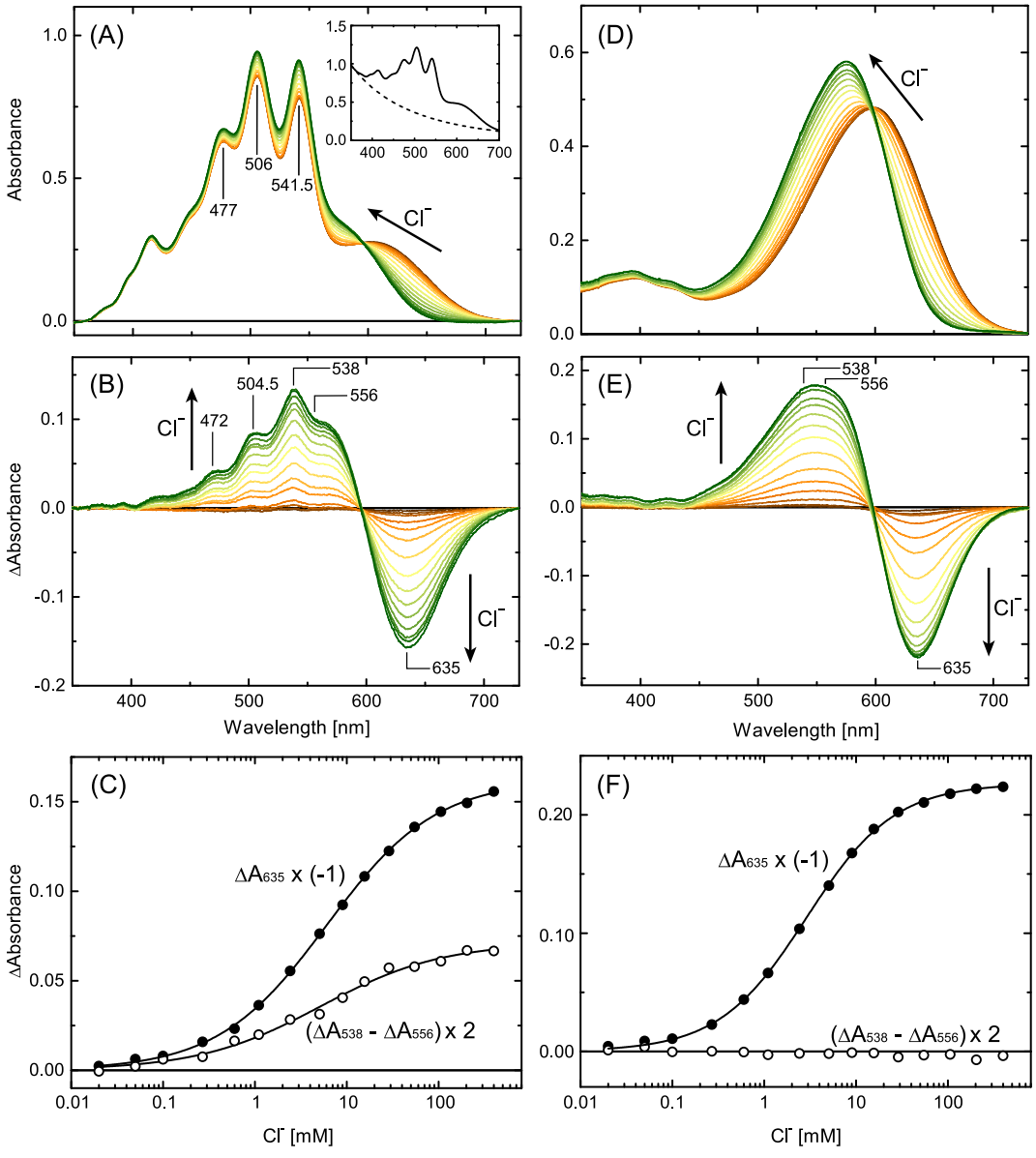

Fig. 3. Cl^--induced absorbance changes of NpHR in the dark state. The left panels (A–C) are the results for the KM-1 membrane fragment. The buffer solution was 50 mM HEPES, pH 7.0, containing 0.01% DDM, 133 mM Na_2SO_4 and 0–400 mM NaCl. In Panel A, the spectra are shown after subtraction of the scattering contribution, which was estimated as described in the inset (see Materials and methods section). The calculated difference spectra from the Cl^- free state are shown in Panel B. The absorbance changes at 635 nm (ΔA_{635}) and the differences between ΔA_{538} and ΔA_{556} (ΔA_{538}–ΔA_{556}) were derived from Panel B, and they are plotted in Panel C against Cl^- concentration by multiplying by "−1" for ΔA_{635} and "2" for ΔA_{538}–ΔA_{556}, respectively. These corresponding results for NpHR purified from *E. coli* cells are shown in the right panels (D–F). The buffer solution was 10 mM MES, pH 6.0, containing 0.1% DDM, 133 mM Na_2SO_4 and 0–400 mM NaCl. In Panel D, absorption spectra are shown without the scattering subtraction. The smooth lines in Panels C and F are the calculated best-fit curves using Eq. (2). The determined parameter values were as follows: Panel C, K_d = 6.1 mM and n = 0.73 for ΔA_{635}; K_d = 5.7 mM and n = 0.74 for ΔA_{538}–ΔA_{556}; Panel F, K_d = 2.9 mM and n = 0.91, respectively.

the crystallographic structure revealed that there exist at least other two Cl^- binding sites [11,31]. The second site (denoted as "Site II" in Fig. 2) is located near the CP end of Brub and is surrounded by the sidechains of Lys65 in one NpHR monomer and Lys148 of a neighboring NpHR. The third site (referred to hereafter as Site III) is located between the B–C loop and F–G loop of NpHR at the EC surface. The Cl^- at Site III is not shown in Fig. 2 because this site is not clearly defined due to its weak affinity [31]. To evaluate the relationship between the Brub spectral changes and Cl^- binding, we performed Cl^- titrations to the claret membrane suspension. The results were summarized in the left panels of Fig. 3. The spectra of the claret membrane included large scattering artifacts (Fig. 3A inset) which slightly changed with changing NaCl concentration. Thus, we evaluated the scattering as shown by the broken line in the inset of Fig. 3A (see Materials and methods section) and displayed the spectra after subtraction of the scattering (Panel A). The calculated difference spectra are shown in Panel B, in which the spectrum of the Cl^--free state has been used as the baseline. For comparison, the corresponding results for NpHR without Brub were shown in the right panels. This NpHR in DDM-solubilized state was prepared from the recombinant *E. coli* cells and thus did not form complexes with Brub. The solubilized NpHR is known to be in a trimeric state like in the KM-1 membrane, albeit without Brub [37]. In Panel D, the spectra at varying Cl^- concentration are shown without scattering subtraction and their difference spectra are shown in Panel E. As shown in Panel E, a Cl^- induced blueshift in the NpHR spectrum results in smooth bilobes in the 450–720 nm region with an isosbestic point at 597 nm. On the other hand, the difference spectra for NpHR with Brub (Panel B) show additional small peaks on the positive lobe, indicating the change of Brub spectrum. In the original spectra shown in Panel A, the three sharp bands from Brub appear at around 477, 506 and 541.5 nm. On the other hand, the peaks due to Brub in Panel B appear at 472, 504.5 and 538 nm, which are 1.5–5 nm lower than the peak positions in the original spectra. This implies that Brub causes a slight blueshift upon increasing Cl^- concentration. To evaluate the relationship between the spectral change of Brub and Cl^- binding, the plots in Panels C and F were made from Panels B and E, respectively. In Panels C and F, the absorbance changes at 635 nm (ΔA_{635}) and the differences between ΔA_{538} and ΔA_{556} (ΔA_{538}–ΔA_{556}) are plotted against Cl^- concentration by multiplying by "−1" for ΔA_{635} and "2" for ΔA_{538}–ΔA_{556}, respectively. Brub has little absorbance above 600 nm. Thus, ΔA_{635} purely reflects the absorbance changes of NpHR due to Cl^- binding to Site I. This assertion was proved by the fitting results: both ΔA_{635}'s in Panels C and F were simulated well by Eq. (2) for the single Cl^- binding site. The K_d for NpHR with Brub (6.1 mM) was approximately 2-fold greater than that of NpHR without Brub (2.9 mM). The K_d in the KM-1 membrane might be influenced by the surface charges of the surrounding lipids. On the other hand, a notable difference is observed in ΔA_{538}–ΔA_{556} between in the presence and absence of Brub. For NpHR with Brub (Panel C), ΔA_{538}–ΔA_{556} increased as the Cl^- concentration increased. In contrast, ΔA_{538}–ΔA_{556} for NpHR without Brub (Panel F) was negligible and independent of the Cl^- concentration. Thus, ΔA_{538}–ΔA_{556} purely reflects the absorbance change of Brub. For NpHR with Brub, the increase of ΔA_{538}–ΔA_{556} almost matches the increase of ΔA_{635}. Actually, K_d determined from ΔA_{538}–ΔA_{556} was 5.7 mM, which is very close to the value from ΔA_{635} (6.1 mM), indicating that Brub changes its absorption spectrum in response to the Cl^- binding to the Site I. In other words, Cl^- binding to Sites II and III cannot be detected by the change in Brub. As described above, Site II is located at the CP end of Brub, and so Cl^- binding to Site II could have significant impact on the Brub spectrum. Thus, Site II probably does not bind Cl^- in aqueous suspension. Supporting results were reported from the molecular dynamics simulation by Jardón-Valadez et al., where the crystal structure shown in Fig. 2 was used as the starting coordinate [38]. Within the first ns of trajectory, the Cl^- at Site II moved away into aqueous medium, whereas the Cl^- at Site I remained close to its original position.

3.2. Brub spectral change during the NpHR photocycle

Next, we performed the flash-photolysis experiments on the KM-1 membranes to detect the Brub spectral changes during the NpHR photocycle. In the dark state, Cl^- binding to Site I causes the spectral change of Brub. On the other hand, flash-induced release of Cl^- should cause the opposite spectral change of Brub. Fig. 4 shows the flash-induced absorbance changes of KM-1 membrane at four Cl^- concentrations. The top panels show the time-dependent absorbance changes at three typical wavelengths. At 500 nm, L_1, L_2 and N are mainly observed. At 580 and 640 nm, the original NpHR and O are mainly observed, respectively. The panels in the second and third rows are the light-dark difference spectra in two time regions and are separated by the time for the maximum accumulation of O. In our apparatus, the K intermediate is not clearly observed due to its fast decay. Thus, the first observed intermediate is L_1, which corresponds to the positive peaks at approximately 500 nm in the panels in the second row. The negative peaks at approximately 580 nm in the same panels are due to the disappearance of the original NpHR by the flash excitation. Over time, the peak at approximately 500 nm decreases with a concomitant increase of the peak at approximately 640 nm, which reflects the accumulation of O. It is noteworthy that the small peaks due to Brub appeared at 450–550 nm as O accumulation increased. Then, these peaks disappeared almost simultaneously as O accumulation disappeared, as shown in the panels in the third row. For comparison, the flash-induced absorbance changes of NpHR without Brub are shown in the left panels of Fig. S1, where small peaks are never observed and the difference spectra are smooth at all times. Brub might change its spectrum by the photoreaction of Brub itself. However, this possibility was ruled out by observation using red flashes shown in right panels of Fig. S1. The peaks due to Brub were also appeared by actinic flashes longer than 580 nm where Brub has no absorption. Thus, Brub causes spectral change in response to the photoreaction of NpHR. As shown in Fig. 4, O accumulation decreases with increasing Cl^- concentration (from left to right columns). Concomitantly, the peaks due to Brub also decreased. These results imply that O formation is associated with Cl^- movement from Site I.

To clearly show which intermediate induces the spectral change of Brub, we analyzed the flash-induced absorbance changes according to the sequential irreversible model. In this analysis, data at all measuring wavelengths were fit simultaneously to the multiexponential function. Previously, we showed that the photocycle of NpHR was adequately described with a 4 exponential function, which indicated the existence of four kinetically distinguishable intermediates (P_i, $i = 1$–4). This result was also valid for NpHR in the KM-1 membrane fragments at any Cl^- concentrations. The final obtained P_i spectra are shown in the bottom panels of Fig. 4 together with the spectrum of the unphotolyzed dark state (P_0). The corresponding decay rate constants of the P_i states are summarized in Fig. S2. It is noteworthy that in the spectra of the P_3 state, small peaks due to Brub were clearly apparent. The P_3 state is the quasi-equilibrium between N (a short wavelength product) and O (a long wavelength product), and this equilibrium shifts from O to N with increasing the Cl^- concentration. Careful inspection indicates that the peaks due to Brub become small as the Cl^- concentration increases. Thus, the spectral change of Brub is probably associated with O and not with N. These results are consistent with the idea that O is the Cl^- releasing state. The precursors P_1 and P_2, which correspond to L_1 and L_2, respectively, do not contain the contributions of Brub in their spectra. On the other hand, the last product P_4, which mainly corresponds to NpHR′, has small but distinct peaks due to Brub in its spectrum. This implies that at NpHR′, the position of captured Cl^- from EC side and/or the conformation of NpHR are not fully restored to those in the original dark state.

3.3. Membrane potential dependence of the NpHR photocycle

The Cl^- transfer is composed of three processes: Cl^- displacement inside the protein, Cl^- release to the CP medium and Cl^- uptake from

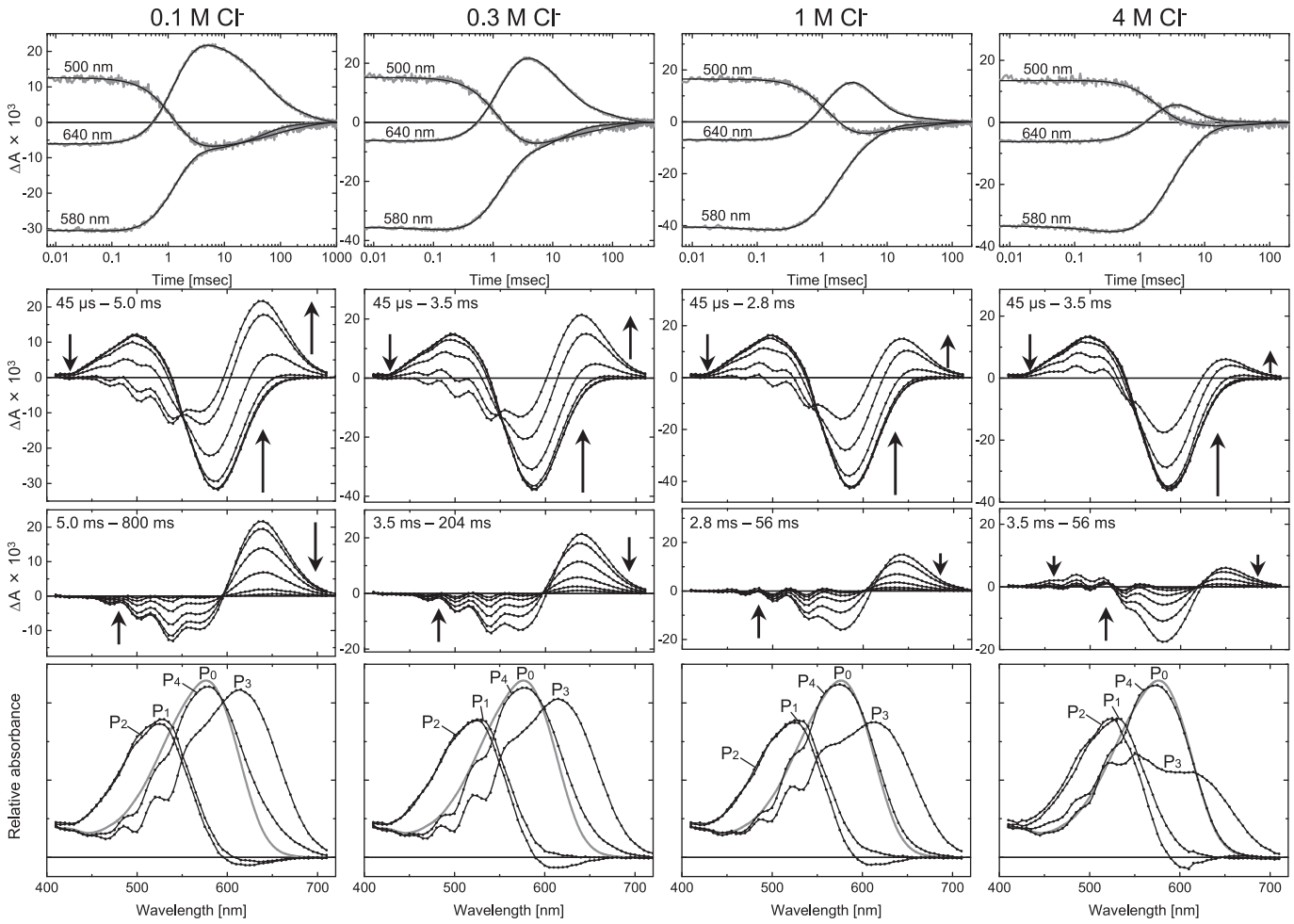

Fig. 4. Flash-induced absorbance changes of the KM-1 membrane fragment at four Cl^- concentrations. The buffer solutions are 50 mM HEPES, pH 7.0, including various concentrations of NaCl. The top panels show the time-dependent absorbance changes at three typical wavelengths, which are denoted in the panels. The smooth lines are the best-fit results to a four exponential function. The panels in the second and third rows show the light minus dark difference spectra in two time regions, which are separated by the time of the maximum accumulation of O. The spectra are collected on a logarithmic time scale. The bottom panels show the calculated absolute spectra of kinetically defined states P_1–P_4 and the spectrum of the unphotolyzed state P_0 (gray thick line). The determined rate constants of these states are plotted in Fig. S2.

the EC medium. These processes could be affected by the imposed membrane potential. Thus, we examined the membrane-potential effect on the photocycle using the cell-envelope vesicles. The KM-1 cells overexpress NpHR and, thus, NpHR-enriched cell-envelope vesicles could be obtained. These were used in the flash-photolysis experiments to produce data with sufficient S/N ratios. We prepared the cell-envelope vesicles by a freeze–thaw method and loaded them with 3.3 M KCl. These vesicles showed high Cl^- pumping activity upon light irradiation (data not shown). Their right-side-out ratio was approximately 70% of the total vesicles, which was checked by the menadione/NADH method [33]. For the flash-photolysis experiments, the vesicles were diluted 100 times into 3.3 M NaCl. Then, a potassium ionophore, valinomycin, was added to induce a potassium diffusion potential of about −118 mV (see Materials and methods section). Even in the absence of valinomycin, a small negative potential is probably imposed because the laser flashes and the monitoring light activates the NpHR in the cuvette. To carry out measurements at a 0 mV membrane potential, TPT and CCCP were added to the vesicle suspension instead of valinomycin. Fig. 5 shows the time-dependent absorbance changes at three typical wavelengths at −118 mV and 0 mV membrane potentials. Independently, it was confirmed that valinomycin, CCCP and TPT did not affect the photocycle observed for the KM-1 membrane fragment

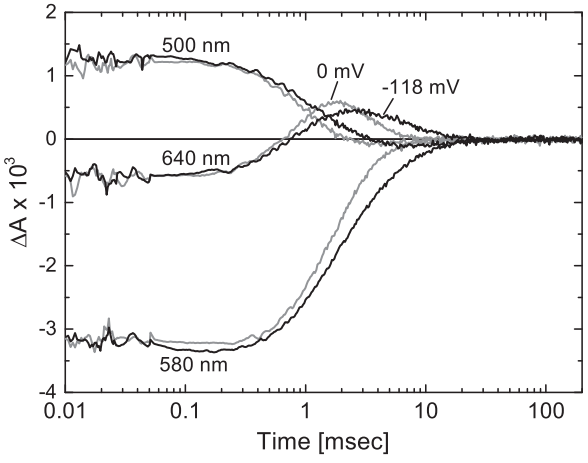

Fig. 5. Membrane-potential induced modulation of the NpHR photocycle. Flash-induced absorbance changes were measured for the KM-1 membrane vesicles, and the time-traces at three typical wavelengths are shown here. The membrane potential of −118 mV was imposed by potassium diffusion in the presence of valinomycin. For the membrane potential of 0 mV, TPT and CCCP were added to cancel the potential imposed by the activation of NpHR.

(data not shown). Thus, the modification of the photocycle was only caused by the imposed membrane potential. The most prominent effect appeared in the time course of O, whose accumulation is observed at 640 nm: The negative membrane potential caused accumulation of O to become small and its decay to slow down. These flash-photolysis data were analyzed with the same procedure described above. Even in the presence of an induced membrane potential, the photocycle was described by the P_1–P_4 states. Their absolute spectra are shown in Fig. 6 together with those at 0 mV. A distinct membrane potential dependence appeared in P_3 state. The N–O quasi-equilibrium was shifted to N by the negative membrane potential. This result implies that the N to O transition is the Cl^- releasing process, which is hindered by the negative membrane potential. The other spectra (P_1, P_2 and P_4) were independent of the membrane potential. This result is consistent with these states containing the physically defined intermediates, L_1, L_2 and NpHR′, respectively. As described above, at lower Cl^- concentration, P_4 includes a contribution of O. This contribution becomes negligible at high Cl^- concentration (3.3 M). The determined decay rate constants of P_i states (k_i) are summarized in Table 1. The negative membrane potential clearly slowed down the decay of P_3 state (k_3, −22%), which corresponds to the formation of NpHR′, the P_4 state. In the previous reports, the formation of NpHR′ was assigned to the Cl^- uptake from the EC medium [14,20]. In addition to this Cl^- movement, the shift of the N–O equilibrium in the P_3 state might relate to the deceleration of P_3 decay, which will be discussed below.

Table 1
Decay rate constants of P_i states in the absence and presence of an imposed interior negative membrane potential.

	0 mV [ms^{-1}]	−118 mV [ms^{-1}]	Change in %[a]
k_1	2.6	2.7	+2.3
k_2	1.4	1.4	+1.3
k_3	0.55	0.43	−22
k_4	0.075	0.068	−9.0

[a] The changes from the values at 0 mV are shown in percent.

4. Discussion

4.1. Opposite-directed spectral changes of Brub observed for the unphotolyzed and photolyzed NpHR states

In the dark state, Brub caused spectral change in response to the Cl^- binding to Site I. During the photocycle, this Cl^- should be moved and then released to the CP medium. Cl^- displacement out of Site I should cause the opposite-directed spectral change of Brub. After the flash irradiation, Brub changed its spectrum almost synchronously with the O formation (see Fig. 4). Fig. 7 contains the plots that compare the spectral changes of Brub in the dark state and during the photocycle. Here, the four data shown in Figs. 3, 4 and Fig. S1 are replotted together. The data 1 and 2 are the results for the KM-1 membranes: 1, the spectral change upon the Cl^- binding to NpHR at the dark state, and 2, the flash-induced spectral change when the accumulation of O reaches the maximum. Data 3 and 4 are the corresponding spectral changes in the absence of Brub. Above 600 nm, Brub has no absorption. Thus, the data without Brub (3 and 4) are plotted after being multiplied by appropriate coefficients to superimpose these data above 600 nm onto the corresponding data with Brub (1 and 2), respectively. The vertical lines are guides to show the peak positions due to Brub. As shown here, the peak shapes are almost opposite between the data 1 and 2, indicating that the spectral changes of Brub are opposite between them. The difference between 1 and 3 indicate that, upon the Cl^- binding to unphotolyzed NpHR, the absorbance of Brub increases at the solid line positions and decreases at the broken line positions, respectively. During the photocycle, Brub causes the opposite absorbance change, which are deduced from the difference between 2 and 4. In this case, Brub decreases its absorbance at the solid line positions and increases at the broken line positions, respectively. These absorbance changes of Brub are schematically shown by the upward and downward arrows in the figure. The opposite-directed spectral changes of Brub indicate that, during the photocycle, Brub changes its spectrum in response to Cl^- displacement from Site I.

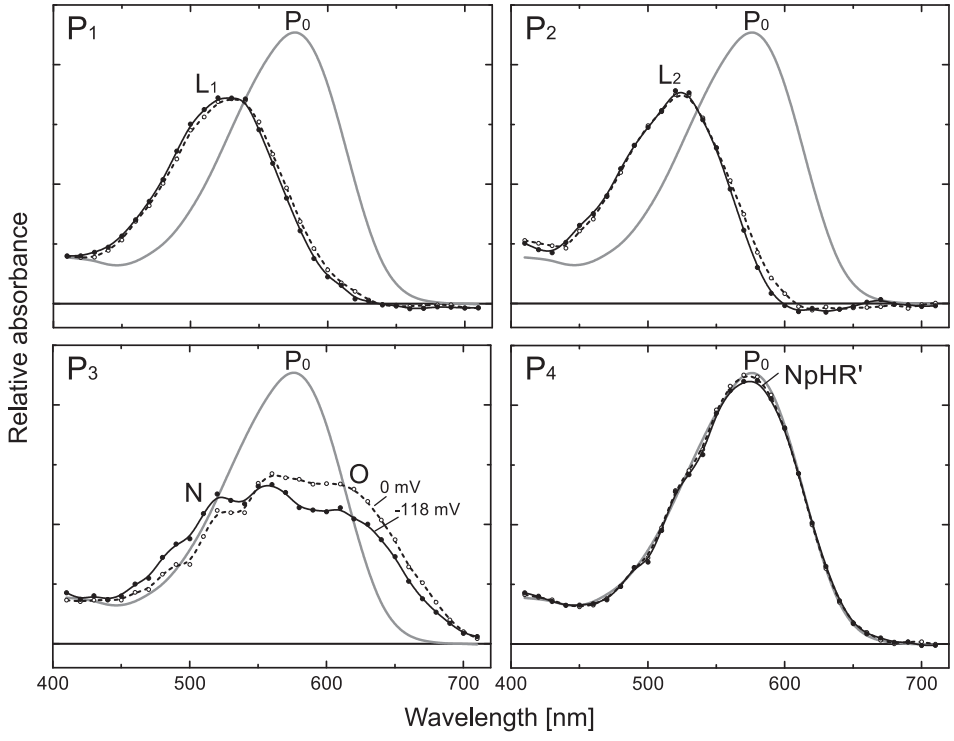

Fig. 6. Membrane-potential induced modulation of the spectra of the P_i states. The calculated absolute spectra of the P_i states at 0 mV (open circles and broken line) and −118 mV (filled circles and solid line) are shown together with the spectrum of unphotolyzed state P_0 (thick gray line).

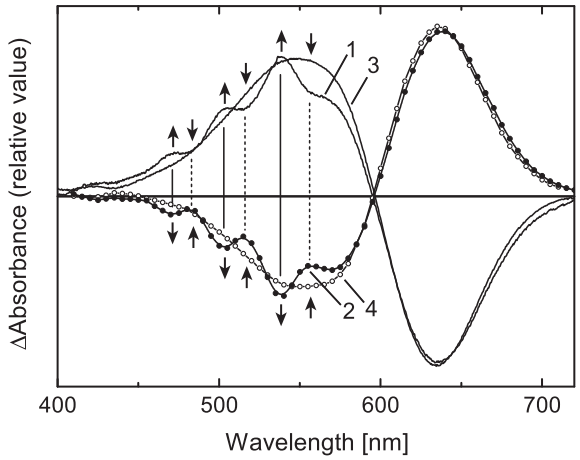

Fig. 7. Directions of the change in the Brub spectra in the dark state and during the photocycle. Four absorbance changes shown in Figs. 3, 4 and S1 are replotted: 1, the absorbance change of KM-1 membrane by the addition of 400 mM Cl^- in the dark state; 2, the flash-induced absorbance change of KM-1 membrane at 5 ms in the presence of 0.1 M Cl^-; 3, the absorbance change of NpHR purified from *E. coli* by the addition of 400 mM Cl^- in the dark state and plotted here multiplied by 0.73; 4, the flash-induced absorbance change of NpHR purified from *E. coli* at 2.2 ms in the presence of 25 mM Cl^- and plotted here multiplied by 0.80. The vertical lines are guides to show the peak positions due to the spectral change of Brub.

4.2. Brub spectral change is associated with O but not with N

As shown in the bottom panels of Fig. 4, the Brub spectral change appeared in the P_3 state. Because P_3 is the quasi-equilibrium between N and O, further analysis was performed to clearly show which intermediate (N or O) involves the spectral change of Brub. In Fig. 8A, the P_3 spectra at four Cl^- concentrations were replotted. The isosbestic point at approximately 550 nm indicates the transition between the two components, N and O. In Panel B, the relative absorbance at 640 nm is plotted against Cl^- concentration. At longer wavelengths, only O has absorbance, and so this plot represents the mole fractions of O of P_3 state. Indeed, this plot was well fit by assuming a single order binding by Cl^-: $N \leftrightarrow O + Cl^-$. The determined K_d is 3.7 M. This successful fitting itself suggests O to be the Cl^- free state. The K_d of 3.7 M is larger than the K_d of approximately 1 M, which was determined for the DDM-solubilized state [20]. The K_d for Cl^- release might be affected by the surrounding environment. At 0.1 M Cl^- ($\ll K_d = 3.7$ M), the mole fraction of O is close to 1. Thus, spectral change of Brub definitely occurs at O; namely, the P_3 spectrum at 0.1 M Cl^- consists of the spectrum of O and spectral change of Brub at O. The sum of these spectral components is hereafter referred to as "$O + \Delta Brub_O$". The following calculations were carried out to examine whether the spectral change of Brub also occurs at N. Panels C and D show the decompositions of the P_3 spectra at 1 M NaCl (P_{3_1M} in Panel C) and 4 M NaCl (P_{3_4M} in Panel D) into the spectra attributable to N and O. From Panel B, the mole fractions of O at 1 M and 4 M Cl^- are determined to be 0.79 and 0.48, respectively. Thus, we can calculate the "$O + \Delta Brub_O$" at these Cl^- concentrations from the $P_{3\_0.1M}$ spectrum by multiplying 0.79 for 1 M Cl^- and 0.48 for 4 M Cl^-, respectively. Then, the spectrum attributable to N, "$N + \Delta Brub_N$", are determined by the subtraction of the "$O + \Delta Brub_O$" from the corresponding P_3 spectra. These spectra attributable to N and O are shown in Panels C and D. It is noteworthy that at both Cl^- concentrations, the spectral change of Brub was associated with O but not with N; namely, $\Delta Brub_O \neq 0$ but $\Delta Brub_N = 0$. This result means that O formation involves the large Cl^- displacement from Site I. As proposed previously [14], this displacement probably corresponds to the Cl^- release to the CP medium. On

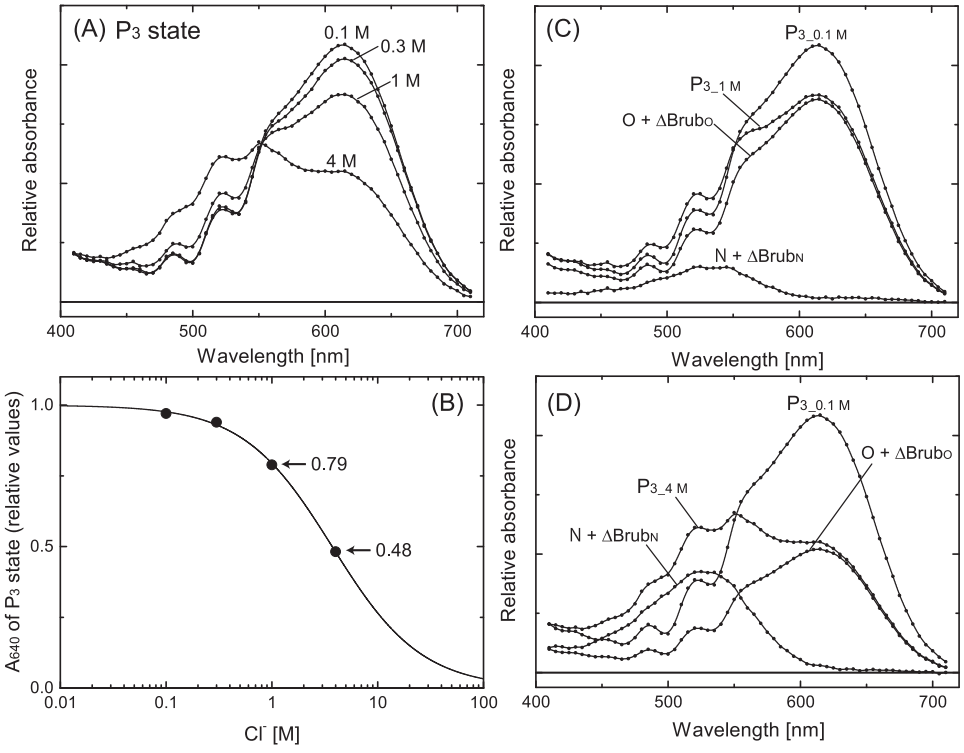

Fig. 8. Decompositions of the P_3 spectra. (A) Cl^- concentration dependence of the P_3 spectra, which were already shown in the bottom panels of Fig. 4. (B) Relative absorbance at 640 nm of the P_3 states are plotted against Cl^- concentration. This plot represents the mole fraction of O constituting the P_3 state. The smooth line is the calculated best fit-curve assuming single order Cl^- binding: $N \leftrightarrow O + Cl^-$. The determined K_d is 3.7 M. Panels (C) and (D) are the decompositions of the P_3 spectra at 1 M Cl^- (C) and 4 M Cl^- (D) into the spectra attributable to the N and O intermediates. These spectra involve small peaks at 450–550 nm if these intermediates induce the spectral changes of Brub. The lines labeled "P_{3_1M}" and "P_{3_4M}" are P_3 spectra at 1 M and 4 M Cl^-, respectively. The spectra attributable to O (labeled "$O + \Delta Brub_O$") were calculated from P_3 spectrum at 0.1 M (labeled "$P_{3\_0.1M}$") by multiplying 0.79 for 1 M Cl^- and 0.48 for 4 M Cl^-, respectively, whose values were determined from Panel B. Then, the spectra attributable to N (labeled "$N + \Delta Brub_N$") were calculated by the subtraction of spectral components of O from the respective P_3 spectra.

the other hand, in the N intermediate, Cl^- probably still exists in the vicinity of Site I.

4.3. O forms from N and decays to NpHR′

N and O appear simultaneously in the P_3 state. In our previous analysis on DDM-solubilized NpHR [20], thus, an uncertainty remained in the sequential order of N and O. To determine this order, we had taken into account a faint contribution of O in the P_4 spectrum. This contribution seems larger for the KM-1 membrane. As shown in the bottom panels of Fig. 4, P_4 spectra contains NpHR′ as the main component and a small contribution of a long wavelength product, which probably corresponds to O. This contribution is prominent at lower Cl^- concentrations, implying the existence of a Cl^--dependent quasi-equilibrium, $O + Cl^- \leftrightarrow NpHR'$. On the other hand, N contribution to P_4 seems not appear at any Cl^- concentration. Thus, NpHR′ probably forms from O, and O forms from N. Moreover, additional evidence was obtained from the appearance of Brub spectral change in the P_4 state. Until 0.3 M Cl^-, the P_4 spectra clearly contain the contribution of O and simultaneously contain the spectral change of Brub. This result is consistent with that $\Delta Brub_O \neq 0$. It is noteworthy that at high Cl^- concentration (1 M and 4 M), P_4 does not contain O while spectral change of Brub appears. This result indicates that the change of Brub spectrum appears in O and remains in NpHR′. Thus, O forms from N and then decays to NpHR′.

4.4. Comparison of the Brub spectral change of O and NpHR′

The P_4 spectrum at 4 M Cl^- consists of the spectrum of NpHR′ and its involved Brub spectral change as described by:

$$P_{4\_4M} = NpHR' + \Delta Brub_{NpHR'} \quad (3)$$

Eq. (3) and the following Eqs. (4)–(7) represent spectral calculations. Because NpHR′ has almost the same spectrum with P_0 state, $\Delta Brub_{NpHR'}$ is estimated by:

$$\Delta Brub_{NpHR'} = P_{4\_4M} - P_0 \quad (4)$$

The calculated $\Delta Brub_{NpHR'}$ is plotted in Fig. 9. On the other hand, the spectrum of P_3 at 0.1 M Cl^- is described by:

$$P_{3\_0.1M} = O + \Delta Brub_O \quad (5)$$

To compare the magnitude of $\Delta Brub_O$ and $\Delta Brub_{NpHR'}$, we calculated the following spectrum:

$$P_{3\_0.1M} - \alpha \times \Delta Brub_{NpHR'} \quad (6)$$

By using Eq. (5), Eq. (6) can be rewritten as

$$O + \Delta Brub_O - \alpha \times \Delta Brub_{NpHR'} \quad (7)$$

The smooth line in Fig. 9 is the calculated result when α is 1.5, which was determined so that the calculated spectrum becomes smooth and does not contain the spectral change of Brub. The smooth spectrum corresponds to the pure spectrum of O. The "smoothness" suggests that the "shapes" of the Brub spectral changes are almost the same between at O and NpHR′, and their magnitudes have the relationship of $\Delta Brub_O = 1.5 \times \Delta Brub_{NpHR'}$. Thus, the larger spectral change of Brub appears in state O, supporting that O is the Cl^- releasing state. During the subsequent O to NpHR′ transition, on the other hand, the Brub spectral change decreases only 33%. This results suggests that NpHR′ is not the simple precursor of the original dark state. A prominent difference should exist between NpHR′ and the dark state. Judging from the absorption spectrum, NpHR′ appears to bind Cl^- around the original Site I. Thus, the spectral change of Brub at NpHR′ might reflect the altered configuration of Brub due to the altered conformation of the neighboring NpHR. Probably, a large conformational change occurs at O and it remains at NpHR′. The recovery from NpHR′ to original dark state (the decay of P_4 state) is the slowest process during the photocycle, which might be due to the substantial difference between the conformations of NpHR′ and the original dark state.

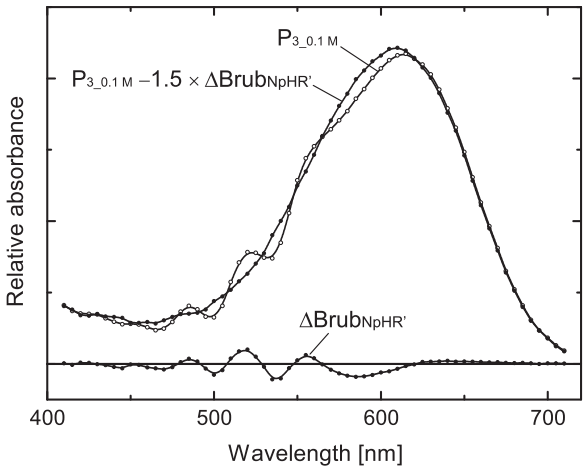

Fig. 9. Calculations to compare the spectral changes of Brub associated with O and NpHR′. The spectral change of Brub ($\Delta Brub_{NpHR'}$) was estimated by the spectral subtraction of P_0 from P_4 at 4 M Cl^-. The absorption spectrum of P_3 state at 0.1 M Cl^- ($P_{3\_0.1\ M}$) consists of the pure spectrum of O and the Brub spectral change at O ($\Delta Brub_O$). The smooth line is the result of spectral calculation "$P_{3\_0.1M} - 1.5 \times \Delta Brub_{NpHR'}$". Note that the peaks due to Brub in $P_{3\_0.1M}$ disappear by this spectral calculation, suggesting $\Delta Brub_O = 1.5 \times \Delta Brub_{NpHR'}$. For details, see text.

4.5. Electrogenic processes during the NpHR photocycle

By using the cell envelope vesicles, we examined the membrane potential-induced modulation of the photocycle. A interior negative membrane potential hinders the inward movement of Cl^-. Previous studies suggested that during the formation of N, Cl^- moves from Site I to the CP channel over the Schiff base [15,19,20]. However, the formation of N, which probably corresponds to the P_2 to P_3 transition, did not slow down when a interior negative membrane potential was imposed (see k_2 values in Table 1). Moreover, formation of N does not involve the spectral change of Brub. From previous studies, we infer that at N, the Cl^- may interact with the OH group of Thr218 because mutations of this residue significantly affect the quasi-equilibrium between N and O [21]. This residue is located only about one helix turn away from the Schiff base. Thus, the Cl^- displacement might be short to cause a significant electrogenicity, which might be a reason of no spectral change of Brub at N.

The prominent effects of the imposed membrane potential appeared in the N–O equilibrium in the P_3 state and its decay rate, k_3. We observed a shift in the N–O equilibrium toward N. This shift is consistent with the N to O transition being associated with Cl^- release to the CP medium. Another observation is the deceleration of k_3. The subsequent P_4 state is regarded to NpHR′ as a main component, which probably binds Cl^- in the vicinity of Site I. The P_3 decay mainly represents the transition rate from O to NpHR′, and so the rate k_3 is described as follows:

$$k_3 = k_0 \times [O] \times [Cl^-] \quad (8)$$

where [O] and [Cl^-] denote the mole fraction of O in P_3 state and the Cl^- concentration in the medium, respectively. The constant k_0 is the proportionality coefficient and depends on the membrane potential if the Cl^- transfer is electrogenic. As described above, [O] also depends on

the membrane potential. The relative absorbance at 640 nm of P_3 state represents [O] (see Fig. 8B). For the P_3 shown in Fig. 6, the relative absorbance at 640 nm decreases approximately 16% upon imposition of the −118 mV membrane potential, indicating that the membrane potential-induced shift of the N–O equilibrium could lower k_3 approximately 16%. On the other hand, the observed decrease of k_3 is approximately 22% (Table 1). Thus, the shift of the N–O equilibrium is the main cause of the deceleration of k_3. The further deceleration is probably caused by a decrease of k_0, reflecting the electrogenicity of the Cl^- transfer in the EC channel. Thus, the membrane potential appears to have significant effects on the Cl^- transfer in the CP channel compared to those in the EC channel. This result might be consistent with previous reports: Ludmann et al. [15] and Muneyuki et al. [19] detected much smaller electrogenicity during the NpHR′ formation compared to that during the O formation. These observations may reflect the difference in dielectric constants of CP and EC channels. As revealed by the crystal structure at the dark state [11], the CP channel mainly consists of hydrophobic residues, while the EC channel consists of many hydrophilic residues and water molecules. The molecular dynamics simulation for the dark state also showed that there are more water molecules in the EC channel than in the CP channel [38]. For the photolyzed state, the CP channel opening and the resultant hydration of the channel were suggested from the FTIR [39] and flash-photolysis studies [21]. Even at this photolyzed state, the CP channel may still have a smaller dielectric constant such that the Cl^- transfer in the channel is more electrogenic compared to that in EC channel. In addition to the dielectric constant, the length of Cl^--transfer pathway can also affect the magnitude of electrogenicity. However, the Cl^- location at N is not clear at present, and so the length for Cl^- release could not be defined. Thus, further studies are required to clarify the molecular origin of the observed effects of the transmembrane potential.

The last rate constant k_4 slightly decreases (−9.0%) by the imposition of the negative membrane potential. This result might reflect the existence of the Cl^- binding site near the EC surface. Previous reports proposed the existence of such a site [17,21]: That is, the Cl^- at the site near the EC surface is transferred to Site I during the O to NpHR′ transition, and then another Cl^- binds to the vacant site near the EC surface during the NpHR′ to original state transition. The final Cl^- binding to the EC surface might involve a small electrogenicity and be delayed by the negative membrane potential. This site might be identical to Site III as describe above. The detailed characterization of this site awaits future studies.

Previously, we examined the membrane voltage dependence of the Cl^- pumping activity under the constant illumination [40], where we expressed NpHR in *Xenopus* oocyte and measured the activity via photo-induced current across the cell membrane. Due to the uphill transport, the pumping activity linearly decreased with increasing negative membrane potential. By imposing a potential of −120 mV, the activity decreased approximately 32% from that at 0 mV. From the standpoint of the turnover rate, the activity should be determined by the slowest rate of k_4 during the photocycle. In the present study, k_4 decreases approximately 9% by the imposition of −118 mV (Table 1). As described above, the right-side-out ratio was approximately 70%. Thus, 9% is probably an underestimate. However, a 32% decrease in the activity is not explained by only the delay of the turnover rate. Another possibility is that the negative membrane potential induces NpHR to return to the original state through a nonelectrogenic pathway. The N–O equilibrium in state P_3 is sensitive to the negative membrane potential and clearly shifts toward N. Thus, the transitions of N to NpHR′ or NpHR might be induced. A previous FTIR study proposed a similar transition in the presence of high concentrations of Cl^-, although the L_2 to NpHR transition was assumed by them [39].

5. Conclusions

We examined the photocycle of NpHR using a mutant strain KM-1, which enabled measurements using Brub as the intrinsic probe. We also conducted these experiments with an imposed interior negative membrane potential. In the dark state, Cl^- binding to Site I induces the Brub spectral change. On the other hand, oppositely directed change of Brub spectrum appeared during the photocycle. The detailed data analysis according to the sequential irreversible model showed that the spectral change of Brub is associated with O and NpHR′ but is not associated with N. This result indicates that O forms from N and decays to NpHR′. Large spectral change of Brub associated with O supports Cl^- release during the N to O transition. Judging from the similar absorption spectra of NpHR′ and the dark state, NpHR′ is already bound by another Cl^- at the vicinity of Site I. Thus, Brub spectral change associating with NpHR′ probably reflects the remaining protein conformational change for the Cl^- release. The imposition of an interior negative potential caused a distinct shift in the N–O quasi-equilibrium toward N. This result also supports the supposition that Cl^- is released during the N to O transition. The membrane potential largely affected the Cl^- releasing process at the CP side, while a smaller effect was observed for the Cl^- transfer in the EC channel. This result might reflect the differences in the dielectric constants of CP and EC channels.

Transparency document

The Transparency document associated with this article can be found, in the online version.

Acknowledgments

This work was supported by grants from the Japanese Ministry of Education, Culture, Sports, Science, and Technology to T.K. (23510251).

Appendix A. Supplementary data

Supplementary data to this article can be found online at http://dx.doi.org/10.1016/j.bbabio.2015.05.002.

References

[1] B. Schobert, J.K. Lanyi, Halorhodopsin is a light-driven chloride pump, J. Biol. Chem. 257 (1982) 10306–10313.
[2] J.L. Spudich, K.-H. Jung, Microbial rhodopsin: Phylogenetic and functional diversity, in: W.R. Briggs, J.L. Spudich (Eds.), Handbook of photosensory receptors, Wiley-VCH Verlag, Weinheim 2005, pp. 1–23.
[3] M. Grote, M. Engelhard, P. Hegemann, Of ion pumps, sensors and channels—Perspectives on microbial rhodopsins between science and history, Biochim. Biophys. Acta 1837 (2013) 533–545.
[4] G. Váró, Analogies between halorhodopsin and bacteriorhodopsin, Biochim. Biophys. Acta 1460 (2000) 220–229.
[5] L.-O. Essen, Halorhodopsin: Light-driven ion pumping made simple? Curr. Opin. Struct. Biol. 12 (2002) 516–522.
[6] A. Duschl, G. Wagner, Primary and secondary chloride transport in *Halobacterium halobium*, J. Bacteriol. 168 (1986) 548–552.
[7] A.V. Avetisyan, A.D. Kaulen, V.P. Skulachev, B.A. Feniouk, Photophosphorylation in alkalophilic halobacterial cells containing halorhodopsin: Chloride-ion cycle? Biochem. Mosc. 63 (1998) 625–628.
[8] M. Falb, F. Pfeiffer, P. Palm, K. Rodewald, V. Hickmann, J. Tittor, D. Oesterhelt, Living with two extremes: Conclusions from the genome sequence of *Natronomonas pharaonis*, Genome Res. 15 (2005) 1336–1343.
[9] A. Matsuno-Yagi, Y. Mukohata, ATP synthesis linked to light-dependent proton uptake in a red mutant strain of *Halobacterium* lacking bacteriorhodopsin, Arch. Biochem. Biophys. 199 (1980) 297–303.
[10] M. Kolbe, H. Besir, L.O. Essen, D. Oesterhelt, Structure of the light-driven chloride pump halorhodopsin at 1.8 Å resolution, Science 288 (2000) 1390–1396.
[11] T. Kouyama, S. Kanada, Y. Takeguchi, A. Narusawa, M. Murakami, K. Ihara, Crystal structure of the light-driven chloride pump halorhodopsin from *Natronomonas pharaonis*, J. Mol. Biol. 396 (2010) 564–579.
[12] S.P. Balashov, Protonation reactions and their coupling in bacteriorhodopsin, Biochim. Biophys. Acta 1460 (2000) 75–94.
[13] J.K. Lanyi, Bacteriorhodopsin, Annu. Rev. Physiol. 66 (2004) 665–688.
[14] G. Váró, R. Needleman, J.K. Lanyi, Light-driven chloride ion transport by halorhodopsin from *Natronobacterium pharaonis*. II. Chloride release and uptake, protein conformation change, and thermodynamics, Biochemistry 34 (1995) 14500–14507.
[15] K. Ludmann, G. Ibron, J.K. Lanyi, G. Váró, Charge motions during the photocycle of *pharaonis* halorhodopsin, Biophys. J. 78 (2000) 959–966.

[16] K. Inoue, M. Kubo, M. Demura, N. Kamo, M. Terazima, Reaction dynamics of halorhodopsin studied by time-resolved diffusion, Biophys. J. 96 (2009) 3724–3734.
[17] J. Guijarro, M. Engelhard, F. Siebert, Anion uptake in halorhodopsin from *Natromonas pharaonis* studied by FTIR spectroscopy: Consequences for the anion transport mechanism, Biochemistry 45 (2006) 11578–11588.
[18] I.V. Kalaidzidis, Y.L. Kalaidzidis, A.D. Kaulen, Flash-induced voltage changes in halorhodopsin from *Natronobacterium pharaonis*, FEBS Lett. 427 (1998) 59–63.
[19] E. Muneyuki, C. Shibazaki, H. Ohtani, D. Okuno, M. Asaumi, T. Mogi, Time-resolved measurements of photovoltage generation by bacteriorhodopsin and halorhodopsin adsorbed on a thin polymer film, J. Biochem. 125 (1999) 270–276.
[20] C. Hasegawa, T. Kikukawa, S. Miyauchi, A. Seki, Y. Sudo, M. Kubo, M. Demura, N. Kamo, Interaction of the halobacterial transducer to a halorhodopsin mutant engineered so as to bind the transducer: Cl^- circulation within the extracellular channel, Photochem. Photobiol. 83 (2007) 293–302.
[21] K. Shibasaki, H. Shigemura, T. Kikukawa, M. Kamiya, T. Aizawa, K. Kawano, N. Kamo, M. Demura, Role of Thr218 in the light-driven anion pump halorhodopsin from *Natronomonas pharaonis*, Biochemistry 52 (2013) 9257–9268.
[22] I. Chizhov, D.S. Chernavskii, M. Engelhard, K.H. Mueller, B.V. Zubov, B. Hess, Spectrally silent transitions in the bacteriorhodopsin photocycle, Biophys. J. 71 (1996) 2329–2345.
[23] I. Chizhov, M. Engelhard, Temperature and halide dependence of the photocycle of halorhodopsin from *Natronobacterium pharaonis*, Biophys. J. 81 (2001) 1600–1612.
[24] G. Váró, L.S. Brown, J. Sasaki, H. Kandori, A. Maeda, R. Needleman, J.K. Lanyi, Light-driven chloride ion transport by halorhodopsin from *Natronobacterium pharaonis*. I. The photochemical cycle, Biochemistry 34 (1995) 14490–14499.
[25] Y. Furutani, K. Fujiwara, T. Kimura, T. Kikukawa, M. Demura, H. Kandori, Dynamics of dangling bonds of water molecules in *pharaonis* halorhodopsin during chloride ion transportation, J. Phys. Chem. Lett. 3 (2012) 2964–2969.
[26] K. Ihara, A. Narusawa, K. Maruyama, M. Takeguchi, T. Kouyama, A halorhodopsin-overproducing mutant isolated from an extremely haloalkaliphilic archaeon *Natronomonas pharaonis*, FEBS Lett. 582 (2008) 2931–2936.
[27] H.S. van Walraven, K. Krab, M.J.M. Hagendoorn, R. Kraayenhof, The use of carotenoids and oxonol VI as probes for membrane potential in proteoliposomes, FEBS Lett. 184 (1985) 96–99.
[28] H.T. Witt, Energy conversion in the functional membrane of photosynthesis. Analysis by light pulse and electric pulse methods. The central role of the electric field, Biochim. Biophys. Acta 505 (1979) 355–427.
[29] J. Otomo, H. Tomioka, H. Sasabe, Properties and the primary structure of a new halorhodopsin from halobacterial strain mex, Biochim. Biophys. Acta 1112 (1992) 7–13.
[30] S.P. Balashov, E.S. Imasheva, V.A. Boichenko, J. Anton, J.M. Wang, J.K. Lanyi, Xanthorhodopsin: a proton pump with a light-harvesting carotenoid antenna, Science 309 (2005) 2061–2064.
[31] S. Kanada, Y. Takeguchi, M. Murakami, K. Ihara, T. Kouyama, Crystal structures of an O-like blue form and an anion-free yellow form of *pharaonis* halorhodopsin, J. Mol. Biol. 413 (2011) 162–176.
[32] J. Hirayama, Y. Imamoto, Y. Shichida, N. Kamo, H. Tomioka, T. Yoshizawa, Photocycle of phoborhodopsin from haloalkaliphilic bacterium (*Natronobacterium pharaonis*) studied by low-temperature spectrophotometry, Biochemistry 31 (1992) 2093–2098.
[33] J.K. Lanyi, R.E. MacDonald, Light-induced transport in *Halobacterium halobium*, Methods Enzymol. 56 (1979) 398–407.
[34] Y. Yamashita, T. Kikukawa, T. Tsukamoto, M. Kamiya, T. Aizawa, K. Kawano, S. Miyauchi, N. Kamo, M. Demura, Expression of *salinarum* halorhodopsin in *Escherichia coli* cells: Solubilization in the presence of retinal yields the natural state, Biochim. Biophys. Acta 1808 (2011) 2905–2912.
[35] M. Sato, T. Kanamori, N. Kamo, M. Demura, K. Nitta, Stopped-flow analysis on anion binding to blue-form halorhodopsin from *Natronobacterium pharaonis*: Comparison with the anion-uptake process during the photocycle, Biochemistry 41 (2002) 2452–2458.
[36] M. Sato, M. Kubo, T. Aizawa, N. Kamo, T. Kikukawa, K. Nitta, M. Demura, Role of putative anion-binding sites in cytoplasmic and extracellular channels of *Natronomonas pharaonis* halorhodopsin, Biochemistry 44 (2005) 4775–4784.
[37] T. Sasaki, M. Kubo, T. Kikukawa, M. Kamiya, T. Aizawa, K. Kawano, N. Kamo, M. Demura, Halorhodopsin from *Natronomonas pharaonis* forms a trimer even in the presence of a detergent, dodecyl-β-D-maltoside, Photochem. Photobiol. 85 (2009) 130–136.
[38] E. Jardón-Valadez, A.N. Bondar, D.J. Tobias, Electrostatic interactions and hydrogen bond dynamics in chloride pumping by halorhodopsin, Biochim. Biophys. Acta 1837 (2014) 1964–1972.
[39] C. Hackmann, J. Guijarro, I. Chizhov, M. Engelhard, C. Rödig, F. Siebert, Static and time-resolved step-scan fourier transform infrared investigations of the photoreaction of halorhodopsin from *Natronobacterium pharaonis*: Consequences for models of the anion translocation mechanism, Biophys. J. 81 (2001) 394–406.
[40] A. Seki, S. Miyauchi, S. Hayashi, T. Kikukawa, M. Kubo, M. Demura, V. Ganapathy, N. Kamo, Heterologous expression of *pharaonis* halorhodopsin in *Xenopus laevis* oocytes and electrophysiological characterization of its light-driven Cl^- pump activity, Biophys. J. 92 (2007) 2559–2569.